

CHEMPHYSCHEM

Supporting Information

On the Synthesis of Chocolate Flavonoids (Propanols, Butanals) in the Interstellar Medium

Matthew J. Abplanalp, Sándor Góbi, Alexandre Bergantini, Andrew M. Turner, and Ralf I. Kaiser*^[a]

cphc_201701350_sm_miscellaneous_information.pdf

Table of Contents

Experimental Procedures (pg. 3)
Results and Discussion: Fourier Transform Infrared Spectroscopy (FTIR) (pg. 4)
Results and Discussion: Photoionization Reflectron Time-of-Flight Mass Spectrometry (PI-ReTOF-MS) (pg. 4)
Results and Discussion: C₃H₈O and C₄H₈O Isomer Yields (pg. 4-5)
Results and Discussion: C₃H₈O and C₄H₈O Isomer Formation Mechanisms (pg. 5-6)
Figure S1 (pg. 7)
Figure S2 (pg. 8)
Figure S3 (pg. 9)
Figure S4 (pg. 10)
Figure S5 (pg. 11)
Figure S6 (pg. 12)
Figure S7 (pg. 13)
Table S1 (pg. 14)
Table S2 (pg. 14)
Table S3 (pg. 15)
Table S4 (pg. 15)
Table S5 (pg. 16)
Table S6 (pg. 16)
References (pg. 17)

Experimental Procedures

The experiments were carried out in an ultrahigh vacuum (UHV) chamber that was evacuated to a few 10^{-11} Torr.^[1] Within the chamber, a silver mirror substrate is interfaced to a cold head (Sumitomo Heavy Industries, RDK-415E), which is connected to a closed cycle helium compressor capable of reaching 5.0 ± 0.1 K. By utilizing a doubly differentially pumped rotational feedthrough (Thermionics Vacuum Products, RNN-600/FA/ MCO) the substrate is able to be rotated in the horizontal plane; utilizing an UHV compatible bellow (McAllister, BLT106) the substrate can be translated in the vertical plane as well. The ice mixtures were prepared by mixing carbon monoxide (CO, Aldrich, 99.99%; ^{13}CO , Aldrich, 99% ^{13}C) and methane (CH_4 , Specialty Gases of America, 99.999%; $^{13}\text{CD}_4$, Isotec, 99% ^{13}C , 99% D) gases in a separate chamber prior to introducing them into the chamber through a glass capillary array at pressures of 5×10^{-8} Torr (Table S1). The deposition of the ice mixture on the silver substrate was monitored with a helium-neon (HeNe) laser (632.8 nm; CVI Melles-Griot; 25-LHP-230); this setup determined the ice thickness to be 480 ± 50 nm via the recorded interference fringes and a refractive index of 1.31 ± 0.02 for the mixed carbon monoxide–methane ice.^[2] These ices were prepared in a ratio of about 3:1 (carbon monoxide : methane) to study the interactions of methane in the presence of an abundance of carbon monoxide, which is typical in interstellar ices. Further studies replicating more realistic ISM ices such as with the incorporation of water and different ice constituent ratios will be needed to investigate the full extent of methane containing ISM ice chemistry. These ice constituents were used as both have been detected in interstellar ices and have been shown to form without energetic processing on dust grains from an icy mantle of simple molecules.^[3]

Each deposited ice was then monitored on line and in situ via a Fourier Transform Infrared (FTIR) spectrometer (Nicolet 6700) continuously throughout the experiment from $6,000\text{--}500\text{ cm}^{-1}$ and a resolution of 4 cm^{-1} every 2 minutes. After the ice was deposited, 5 keV electrons processed the mixture over the $1.0 \pm 0.1\text{ cm}^2$ area at an angle of incidence of 70° to the surface normal of the substrate for 1 hour at a current of 30 nA. Next, Monte Carlo simulations (CASINO) were used to calculate the average penetration depths of $350 \pm 70\text{ nm}$ ($\text{CO}\text{--}\text{CH}_4$) and $300 \pm 60\text{ nm}$ ($^{13}\text{CO}\text{--}^{13}\text{CD}_4$),^[4] which corresponds to a dose of $3.1 \pm 1.0\text{ eV}$ per CO molecule and $3.5 \pm 1.0\text{ eV}$ per CH_4 molecule for the $\text{CO}\text{--}\text{CH}_4$ ice mixture and $4.5 \pm 0.9\text{ eV}$ per ^{13}CO molecule and $3.3 \pm 0.7\text{ eV}$ per $^{13}\text{CD}_4$ molecule for the $^{13}\text{CO}\text{--}^{13}\text{CD}_4$ ice mixture (Table S2). These doses were calculated utilizing the densities of 1.03 g cm^{-3} (CO),^[5] 0.47 g cm^{-3} (CH_4),^[6] 0.68 g cm^{-3} (CD_4).^[7] Note that the energetic electrons simulate the secondary electrons produced in the track of galactic cosmic rays penetrating an interstellar ice.^[8] Quantitatively spoken, the calculated dose in the laboratory simulation experiments represents typical energy depositions equivalent to an exposure of ices in cold molecular clouds over 10^6 years in space.^[9]

After the ice has been irradiated, the controlled heating of the substrate (temperature programmed desorption; TPD) from 5 K to 300 K at a rate of 0.5 K min^{-1} was used to sublimate the processed ice along with any volatile products for the gas phase analysis with the tunable vacuum ultraviolet (VUV) photoionization reflectron time-of-flight mass spectrometry (PI-ReTOF-MS) technique. Here, subliming molecules are ionized via single photon ionization with coherent VUV light at 30 Hz. The VUV generation chamber is operated at a pressure of about 4×10^{-4} Torr and with the backing pressure for the pulse valve at about 2,000 Torr. Non-resonant four-wave mixing was used to generate 10.49 eV (118 nm) photons from the third harmonic of a Nd:YAG laser (354.6 nm; Spectra Physics, PRO-250-30) by frequency tripling in pulsed jets of xenon (Specialty Gases; 99.999%).^[10] The remaining photoionization energies—9.63 eV, 9.75 eV, and 9.93 eV—were produced via resonant four-wave difference mixing ($\omega_{\text{VUV}} = 2\omega_1 - \omega_2$) in krypton (Specialty Gases; 99.999%). As an example, in order to produce the 9.63 eV (128.7 nm; ω_{VUV}) photons, first the necessary ultraviolet (202.3 nm; 6.13 eV; ω_1) and visible (472.1 nm; 2.63 eV; ω_2) wavelengths were generated by a pair of Nd:YAG pumped dye lasers. To generate the ω_1 light the dye laser output (Sirah, Cobra-Stretch; 606.9 nm, 2.04 eV) was frequency tripled using $\beta\text{-BaB}_2\text{O}_4$ (BBO) crystals (44° and 77°). Meanwhile, ω_2 light was the output from the second Nd:YAG pumped dye laser (Sirah, Precision Scan) of 472.1 nm (2.63 eV). After the wavelengths to be mixed are generated they are both temporally and spatially overlapped via a pulse delay generator (Quantum Composers, 9518) and dichroic mirrors or UV prisms, respectively. Next, ω_1 and ω_2 are focused through a UV grade fused silica window (Thorlabs; WG42012) with a convex lens (Thorlabs; LA4579; $f = 300\text{ mm}$) into the VUV generation chamber that is pulsing jets of krypton at 30 Hz and a width of 80 μs , which produces VUV at 9.63 eV to photoionize molecules subliming from the processed ice.^[11] Since multiple resonant and non-resonant processes ($2\omega_1 + \omega_2$; $2\omega_1 - \omega_2$; $3\omega_1$; $3\omega_2$) may be simultaneously occurring in the non-linear medium (xenon; krypton) a bi-convex lithium fluoride lens (LiF; ISP Optics, LiF-L-38.1-3) is used to separate the different wavelengths based on their refractive indices in LiF. This allows for the selection of only the desired wavelength to pass through a 1 mm aperture into the UHV chamber to ionize subliming molecules.

The ions are probed with a reflectron time-of-flight mass spectrometer (Jordan TOF Products, Inc.) and detected, based upon the arrival time, by a multichannel plate (MCP) operating in a dual chevron configuration. The ion signals from the MCP were then shaped, amplified (Ortec 9305), and recorded with a personal computer multichannel scalar (FAST ComTec, P7888-1 E) which is triggered via the pulse delay generator at 30 Hz. Here the ReTOF signal is the average of 3600 sweeps

of the mass spectrum in 4 ns bin widths, which corresponds to an increase in the substrate temperature of 1 K between the ReTOF data points.

Results and Discussion

Fourier Transform Infrared Spectroscopy (FTIR):

The irradiation of the isotopic ice ($^{13}\text{CO}-^{13}\text{CD}_4$) caused several new infrared peaks to appear (Figure S1). These could be assigned to several small molecules as well as functional groups of more complex species (Table S3). One of these newly assigned functional groups belongs to the carbonyl stretch ($^{13}\text{C}=\text{O}$) which is found in several key isomers of interest for this study. Monitoring the carbonyl stretch detected in the processed carbon monoxide–methane ice during TPD (Figure S2) shows that it could be related to the isomers of interest as it decreases in intensity over the temperature range while the ion signals of interest increases. Furthermore, by comparing calibration ices, both pure and 1% mixtures with respect to carbon monoxide and methane, of several isomers (Sigma-Aldrich, *n*-propanol, 99.9%; *i*-propanol, 99.9%; *n*-butanal, 99.5%; *i*-butanal, 99.5%) to the irradiated ice there are several infrared stretches that correspond to infrared stretches observed in the irradiated ice (Figure S3).

Photoionization Reflectron Time-of-Flight Mass Spectrometry (PI-ReTOF-MS):

As noted above, the experiments were conducted using non-isotopic carbon monoxide–methane ($\text{CO}-\text{CH}_4$) ice mixtures, but in order to unambiguously confirm the identity of the several astrophysically relevant species in the gas phase such as $\text{C}_3\text{H}_8\text{O}$ and $\text{C}_4\text{H}_8\text{O}$ the isotopic carbon monoxide–methane ($^{13}\text{CO}-^{13}\text{CD}_4$) ice mixture was needed. This isotopic mixture shifts the ion signal corresponding to $\text{C}_3\text{H}_8\text{O}$ ($^{13}\text{C}_3\text{D}_8\text{O}$; $m/z = 71$) and $\text{C}_4\text{H}_8\text{O}$ ($^{13}\text{C}_4\text{D}_8\text{O}$; $m/z = 84$) to unique positions, where no other molecules overlap with them in the mass spectrum. This isotopic shift coupled with tunable PI-ReTOF-MS resulted in confident assignments of the molecular formulae to ions, but also of specific isomers based on the ionization energies.

To further confirm the assignments to the isomers of interest, calibration experiments of 1% *n*-propanol, *i*-propanol, *n*-butanal, and/or *i*-butanal in carbon monoxide–methane ($\text{CO}-\text{CH}_4$) ices were subjected to the same experimental procedure as described before except that these ices were not irradiated. The ion signals for each of these experiments confirms that *n*-propanol, *i*-propanol, and *n*-butanal will only be ionized at 10.49 eV but not at 9.75 eV (Figure S4A-C). Figure S4D also shows *i*-butanal can be ionized at 10.49 eV and 9.75 eV, with the difference in signal intensity due to the change in photoionization cross section, but that it will not be ionized and therefore not detected at 9.63 eV. Furthermore, the calibration ion signals for *n*- and *i*-propanol and *n*- and *i*-butanal were then overlaid with the ion signals for $m/z = 71$ and $m/z = 84$, respectively, which were recorded from the TPD of the irradiated isotopic carbon monoxide–methane ($^{13}\text{CO}-^{13}\text{CD}_4$) ice (Figure S5). Figure S5A shows that the second peak of the unknown molecule(s) shows a common sublimation onset temperature as the first peak of $m/z = 71$ had begun to return to the baseline at about 127 K. This match shows that the second peak of $m/z = 71$ belongs to *n*- and/or *i*-propanol. As discussed in the main text, the tunable experiments confirm this assignment as the PI energy of 9.93 eV results in a single peak that corresponds only to the first peak observed for $m/z = 71$ at 10.49 eV. Methyl ethyl ether is not commercially available and therefore was not used as a calibration compound. Similarly, Figure S5B shows that both *n*- and *i*-butanal have a similar sublimation onset temperature of 112 K, which matches very closely the rise in the ion signal of $m/z = 84$ corresponding to the unknown molecule(s) from the irradiated isotopic carbon monoxide–methane ($^{13}\text{CO}-^{13}\text{CD}_4$) ice.

$\text{C}_3\text{H}_8\text{O}$ and $\text{C}_4\text{H}_8\text{O}$ Isomer Yields:

Since these ion signals have been unambiguously assigned they will be hereafter referred to with their natural isotopic constituents ($\text{C}_3\text{H}_8\text{O}$ and $\text{C}_4\text{H}_8\text{O}$). The calibration ices were also used to determine the yield per energy deposited of the molecules within the irradiated ice.^[12] First, the number of molecules of the calibration compound in the ice was determined utilizing infrared absorption coefficients.^[13] Next, the calibration ices were sublimed and analyzed with PI-ReTOF-MS (Figure S4). By integrating the ion signal over temperature and correcting for the photoionization cross section of the calibration molecule the number of counts detected via PI-ReTOF-MS can be correlated with the number of molecules in the ice. Using this PI-ReTOF-MS calibration factor and knowing the dose deposited into the ice via 5 keV electrons from the CASINO calculations allows for the yield per energy deposited of individual molecules to be determined from only PI-ReTOF-MS counts corresponding to a molecule and that molecule's PI cross section (Table S4).

To calculate the yields of the $\text{C}_3\text{H}_8\text{O}$ isomers first the yield of methyl ethyl ether ($2.1 \pm 0.9 \times 10^{-5}$ molecules eV^{-1}) was determined by using the PI-ReTOF-MS ion signal at 9.93 eV (Figure 3C), which can only be due to methyl ethyl ether, and methyl ethyl ether's PI cross section at 9.93 eV (4.29 Mb).^[14] The signal due to methyl ethyl ether can then be subtracted

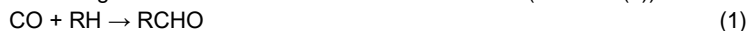
from the ion signal at 10.49 eV (Figure 3B) that could belong to all three C₃H₈O isomers to produce a corrected spectrum that can only be due to *n*- and/or *i*-propanol. As shown in Figure S5 the sublimation profiles of *n*- and *i*-propanol are very similar and Table S4 also shows that their ionization energies (IE) are too similar to selectively ionize only one of the isomers but not the other. Therefore, the yield calculations for *n*- and *i*-propanol were carried out assuming that the ion signal of *m/z* = 71, which was not due to methyl ethyl ether, corresponded to only one of these isomers at a time, this results in an upper limit of $2.2 \pm 0.9 \times 10^{-4}$ molecules eV⁻¹ and $1.2 \pm 0.5 \times 10^{-3}$ molecules eV⁻¹ for *n*-propanol and *i*-propanol, respectively. Although the IEs of *n*- and *i*-propanol are too close to allow selective ionization of these isomers, the *i*-propanol isomer was shown to fragment extensively at 10.49 eV and therefore may contribute only a small amount to the ion signal *m/z* = 71.^[14]

In order to calculate the *n*- and *i*-butanal isomer yields a similar procedure was followed. First, the ion signal corresponding to *m/z* = 84 at 9.63 eV (Figure 3J) is not due to either C₄H₈O isomer and was able to be deconvoluted using only two peaks to fit the signal. The first peak spanned 136–156 K with a maximum at 146 K and the second peak ranged from 88–240 K with a maximum at 164 K. Here, the sublimation profiles of the calibration experiments for both C₄H₈O isomers correspond much more closely to the first deconvolution peak, which follows the typical trend of more polar molecule (alcohols) having a higher sublimation temperature than a less polar isomer (aldehyde) (Figure S5). Therefore, the second of the deconvoluted peaks was then scaled to match the signal detected for *m/z* = 84 at 9.75 eV (Figure 3I) as this peak does not have any interference from the C₄H₈O isomer, *i*-butanal. Next, the scaling factor used to match the second deconvolution peak to the 9.75 eV signal was then applied to the first deconvolution peak as well. If there is any difference between the 9.75 eV signal and the scaled 9.63 eV signal (Figures 3I & 3J), this can be directly related to the *i*-butanal signal. There was in fact a difference in the signals which corresponded to a yield of $2.0 \pm 0.8 \times 10^{-4}$ molecules eV⁻¹ of *i*-butanal. This procedure was repeated to determine the yield of *n*-butanal by deconvoluting the *m/z* = 84 signal at 9.75 eV (Figure 3I) and scaling the second peak to the signal at 9.93 eV (Figure 3H) where the only difference in signals corresponds to *n*-butanal. Again there was a difference and this resulted in a yield of $1.3 \pm 0.5 \times 10^{-4}$ molecules eV⁻¹ of *n*-butanal.

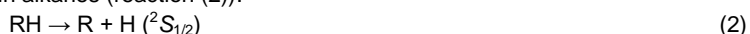
The relative ratios of these isomers (branching ratios) also provide important information on the environment from which they were synthesized. If the isomers were formed from a thermodynamic equilibrium pathway, the branching ratio will be constrained by the equilibrium constant *K* which is defined as the quotient of the isomers' concentrations where $K = [\text{isomer1}]/[\text{isomer2}] = \exp(-\Delta G/RT)$ at a certain temperature (*T*), utilizing the ideal gas constant (*R*), and the difference in standard Gibbs free energies of the isomers (ΔG) (Table S6). The theoretical thermal equilibrium ratios were calculated utilizing temperatures of 10 K and 200 K, with the latter defining the maximum temperature associated with where these isomers of interest were observed to sublime, to be $2.3 \pm 0.4 \times 10^{90}$ (10 K) and of $3.3 \pm 0.6 \times 10^4$ (200 K) for *i*-propanol versus *n*-propanol, $8.5 \pm 0.7 \times 10^{196}$ (10 K) along with $7.0 \pm 0.6 \times 10^9$ (200 K) for *n*-propanol versus methyl ethyl ether, $2.0 \pm 0.1 \times 10^{287}$ (10 K) as well as $2.3 \pm 0.1 \times 10^{14}$ (200 K) for *i*-propanol versus methyl ethyl ether, and $1.9 \pm 0.1 \times 10^{157}$ (10 K) and $7.3 \pm 0.3 \times 10^7$ (200 K) for *i*-butanal versus *n*-butanal (Table S6). However, a comparison of these ratios with the experimentally derived ratios of 6 ± 3 (*i*-propanol : *n*-propanol), 11 ± 6 (*n*-propanol : methyl ethyl ether), 57 ± 32 (*i*-propanol : methyl ethyl ether), and 0.7 ± 0.3 (*i*-butanal : *n*-butanal) shows a significant overproduction of several isomers by 89, 195, 285, and 157 orders of magnitude, respectively. Therefore, the data reveal that in our experiments, these isomers are not formed under thermal equilibrium conditions, but through non-equilibrium processes within the ices.

C₃H₈O and C₄H₈O Isomer Formation Mechanisms:

Having identified at least three COMs – *i*-butanal and *n*-butanal along with *i*-propanol and/or *n*-propanol, we are discussing now possible formation pathways. For simplicity in the following discussion, the ¹³C label is dropped. It should be stressed that although the FTIR analysis provided evidence on the emergence of functional groups associated with aldehydes even at 5 K, the FTIR data were unable to identify individual aldehydes due to overlapping absorptions of the functional groups. Therefore, kinetic profiles linked to the formation of individual COMs could not be provided, and we are discussing possible reaction mechanisms, which have to be verified in future experiments. Aldehydes (RCHO) with R being an alkyl group can be accounted for via the reaction of a single carbon monoxide and alkane molecule (reaction (1)).



However, the overall reaction (1) is often endoergic and therefore thermodynamically unfavorable at 5 K (Table S5). Therefore, this reaction has to be initiated by secondary electrons produced in the track of GCRs within interstellar ices starting with a carbon-hydrogen bond rupture within alkanes (reaction (2)).^[1, 9, 15]



Although this reaction is endoergic of typically 380 – 430 kJ mol⁻¹ (3.94 eV – 4.46 eV) for methane, ethane, and propane (reactions (S3), (S5-S7); Table S5), the electrons processing the ice transfer several electron volts of energy to the hydrocarbon molecule; this energy can be used to cleave this bond. Reaction (2) results in the formation of an alkyl radical (R) as well as a suprathermal hydrogen atom (H) that is able to overcome barriers to addition (*E_b*) such as with carbon monoxide in reaction (3) (*E_b* = 11 kJ mol⁻¹, 0.11 eV; $\Delta_{\text{R}}G = -56$ kJ mol⁻¹, -0.59 eV).



Now, the newly generated alkyl (R) and formyl (HCO) radicals can recombine in the ice barrierlessly (reaction (4); $\Delta_{\text{R}}G = -342 \text{ kJ mol}^{-1}$, -3.54 eV) to form aldehydes such as *n*-butanal (reaction (S10); $\text{CH}_3\text{CH}_2\text{CH}_2\text{CHO}$; $\Delta_{\text{R}}G -328 \text{ kJ mol}^{-1}$, -3.40 eV) and *i*-butanal (reaction (S11); $(\text{CH}_3)_2\text{CHCHO}$; $\Delta_{\text{R}}G -344 \text{ kJ mol}^{-1}$, -3.56 eV ; Table S5).



Aldehydes produced in the ice can take place in further reactions such as hydrogenation to an alcohol (reaction (5)) for example production of *n*-propanol (reaction (S13); $\text{CH}_3\text{CH}_2\text{CH}_2\text{OH}$; $\Delta_{\text{R}}G -485 \text{ kJ mol}^{-1}$, -5.02 eV) or *i*-propanol (reaction (S16); $(\text{CH}_3)_2\text{CHOH}$; $\Delta_{\text{R}}G -472 \text{ kJ mol}^{-1}$, -4.89 eV) involving suprathreshold hydrogen atoms.



The non-equilibrium nature of the formation pathways is further supported by the relative yields of the isomers of interest (Table S6) with branching ratios of 6 ± 3 (*i*-propanol : *n*-propanol), 11 ± 6 (*n*-propanol : methyl ethyl ether), 57 ± 32 (*i*-propanol : methyl ethyl ether), and 0.7 ± 0.3 (*i*-butanal : *n*-butanal). These branching ratios prove that they could have only been synthesized from non-equilibrium pathways within the ices, but not through thermal reactions in the warm up phase, as several isomers are overproduced by orders of magnitude when compared to thermal pathways. It should also be noted that another pathway to form the $\text{C}_3\text{H}_8\text{O}$ alcohol isomers via oxygen (^1D) production from carbon monoxide (reaction (S21); $\Delta_{\text{R}}G = 1260 \text{ kJ mol}^{-1}$, 13.07 eV) followed by insertion into a propane carbon-hydrogen bond (reactions (S22-S23), or carbon-carbon bond (reaction (S24); $\Delta_{\text{R}}G = -548 \text{ kJ mol}^{-1}$, -5.68 eV) is also possible in the current experiment.

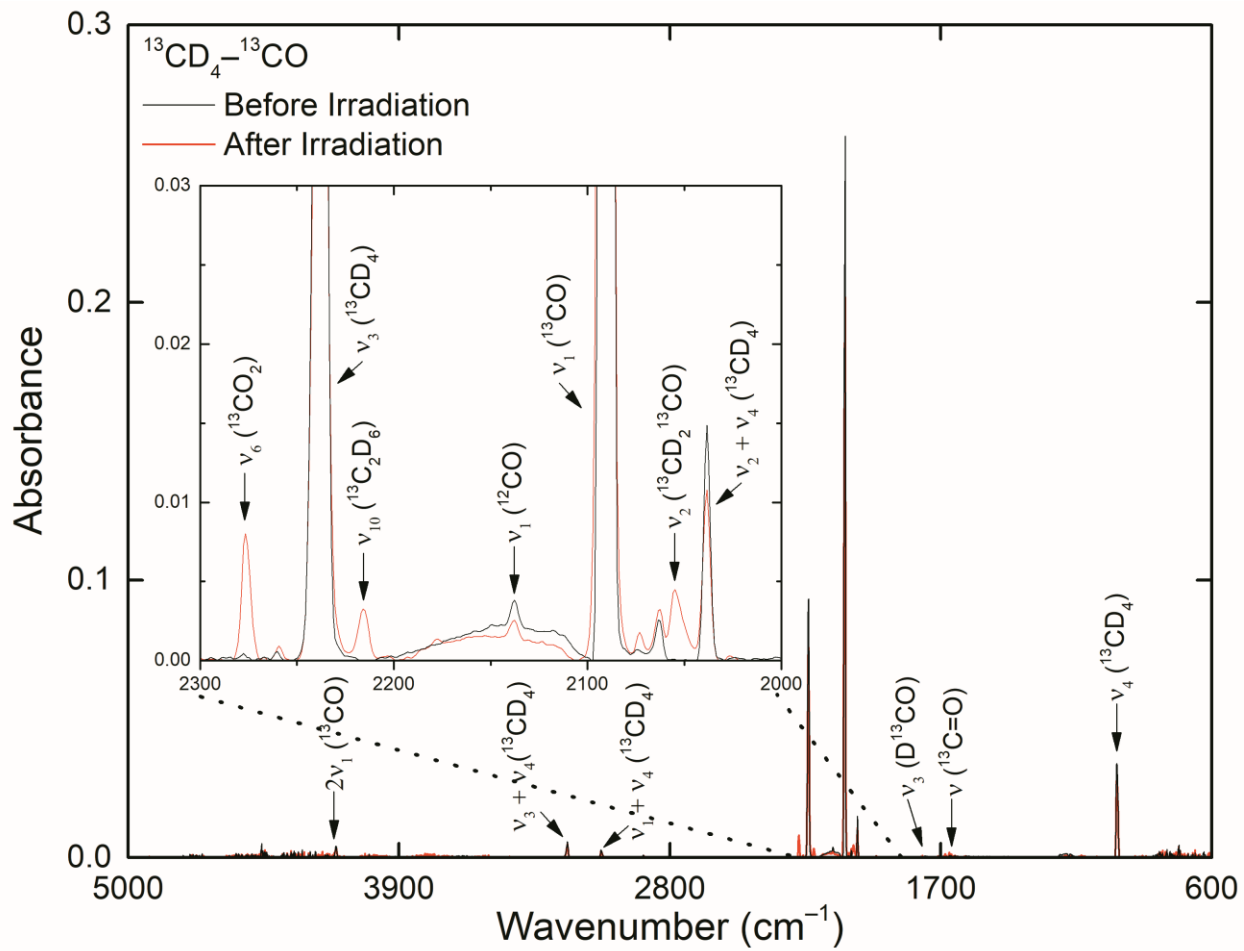


Figure S1. Infrared spectra from 5,000–600 cm^{-1} for methane ($^{13}\text{CD}_4$) and carbon monoxide (^{13}CO) ice before (black) and after (red) the processing along with the assignments.

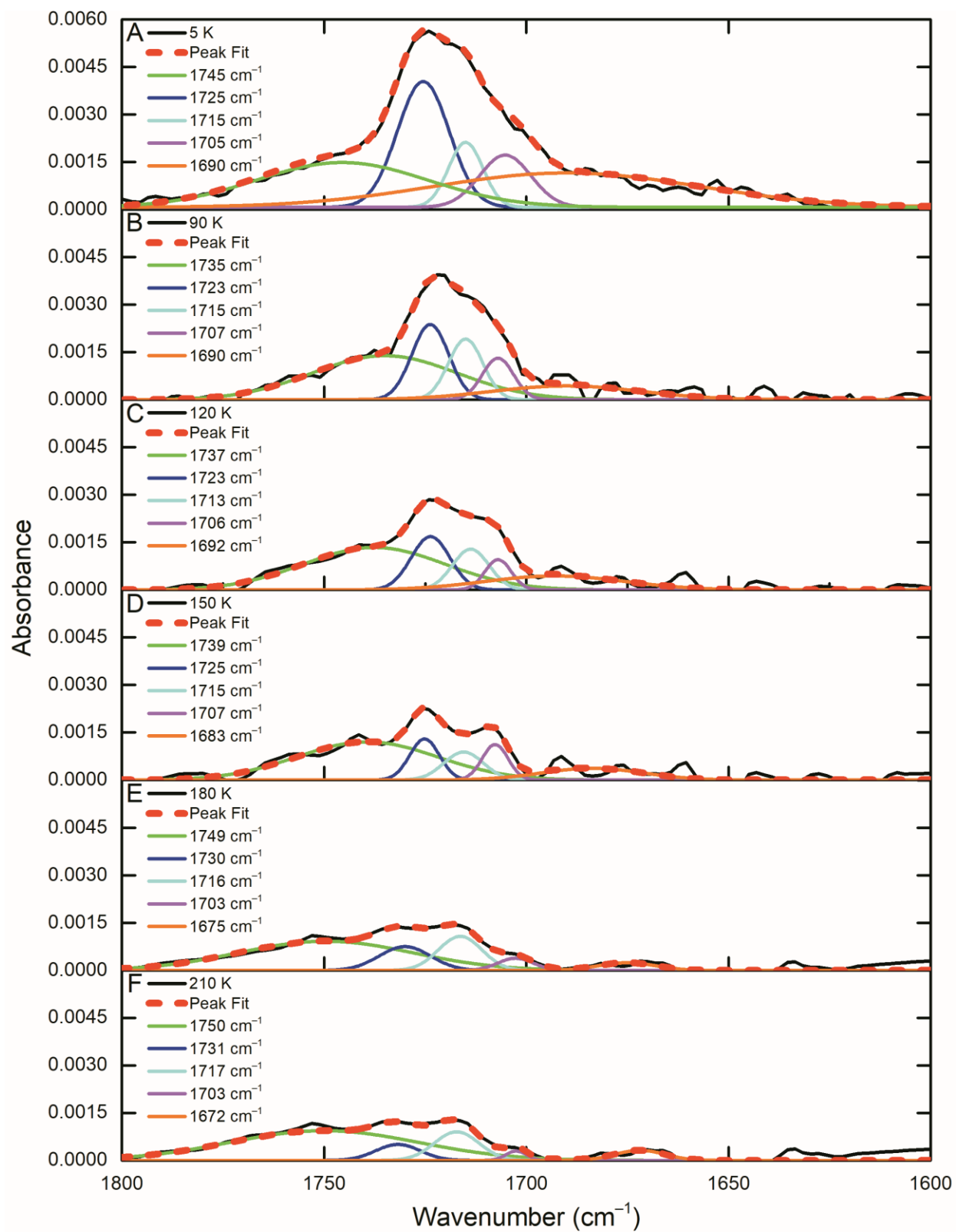


Figure S2. Deconvoluted infrared spectra of carbon monoxide-methane (CO-CH_4) from $1600\text{--}1800\text{ cm}^{-1}$ after irradiation for several TPD temperatures spanning the sublimation event of the isomers of interest (A) 5 K, (B) 90 K, (C) 120 K, (D) 150 K, (E) 180 K, and (F) 210 K.

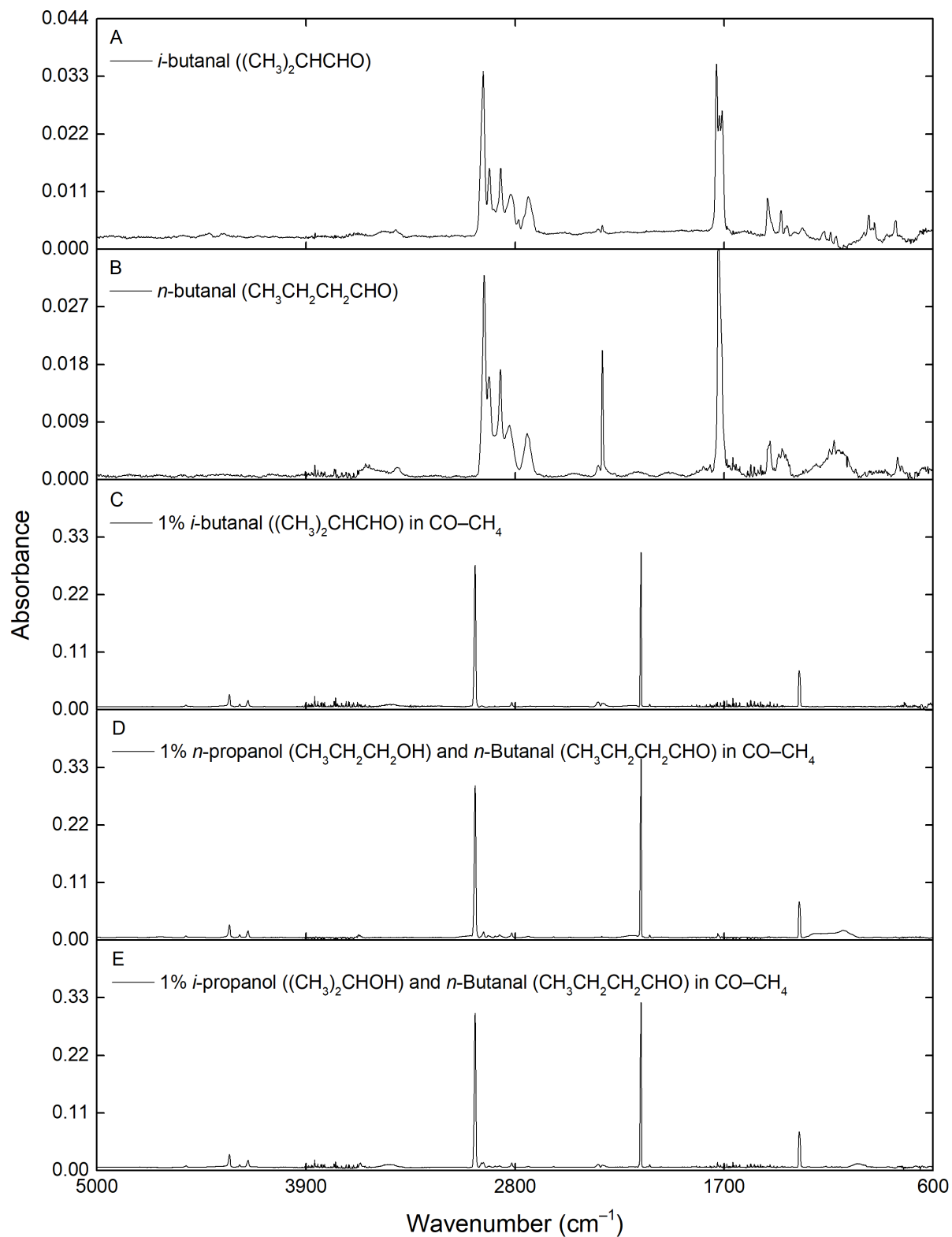


Figure S3. Infrared spectra from 600–5000 cm^{-1} for (A) pure *i*-butanal ice (B) pure *n*-butanal ice (C) 1% *i*-butanal doped carbon monoxide–methane (CO-CH_4) ice (D) 1% *n*-propanol and 1% *n*-butanal doped carbon monoxide–methane ice (E) 1% *i*-propanol and 1% *n*-butanal doped carbon monoxide–methane ice.

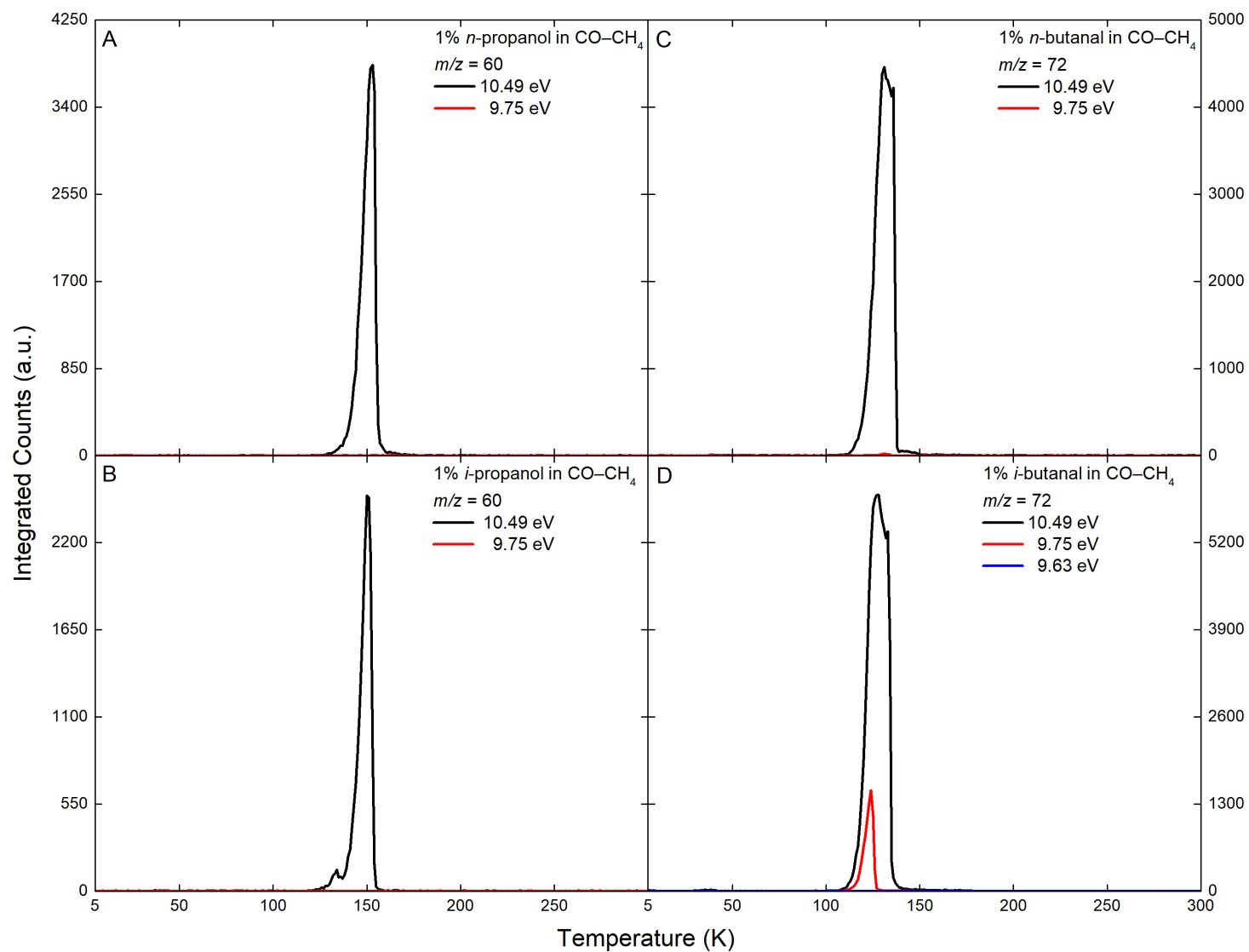


Figure S4. PI-ReTOF-MS data recorded at (A) $m/z = 60$ from separate unirradiated carbon monoxide–methane ice containing 1% of the calibration compound *n*-propanol and (B) *i*-propanol with a PI energy of 10.49 eV. PI-ReTOF-MS data recorded at $m/z = 72$ from separate unirradiated carbon monoxide–methane ice containing 1% of the calibration compound (C) *n*-butanol and (D) *i*-butanol at a PI energy of 10.49 eV.

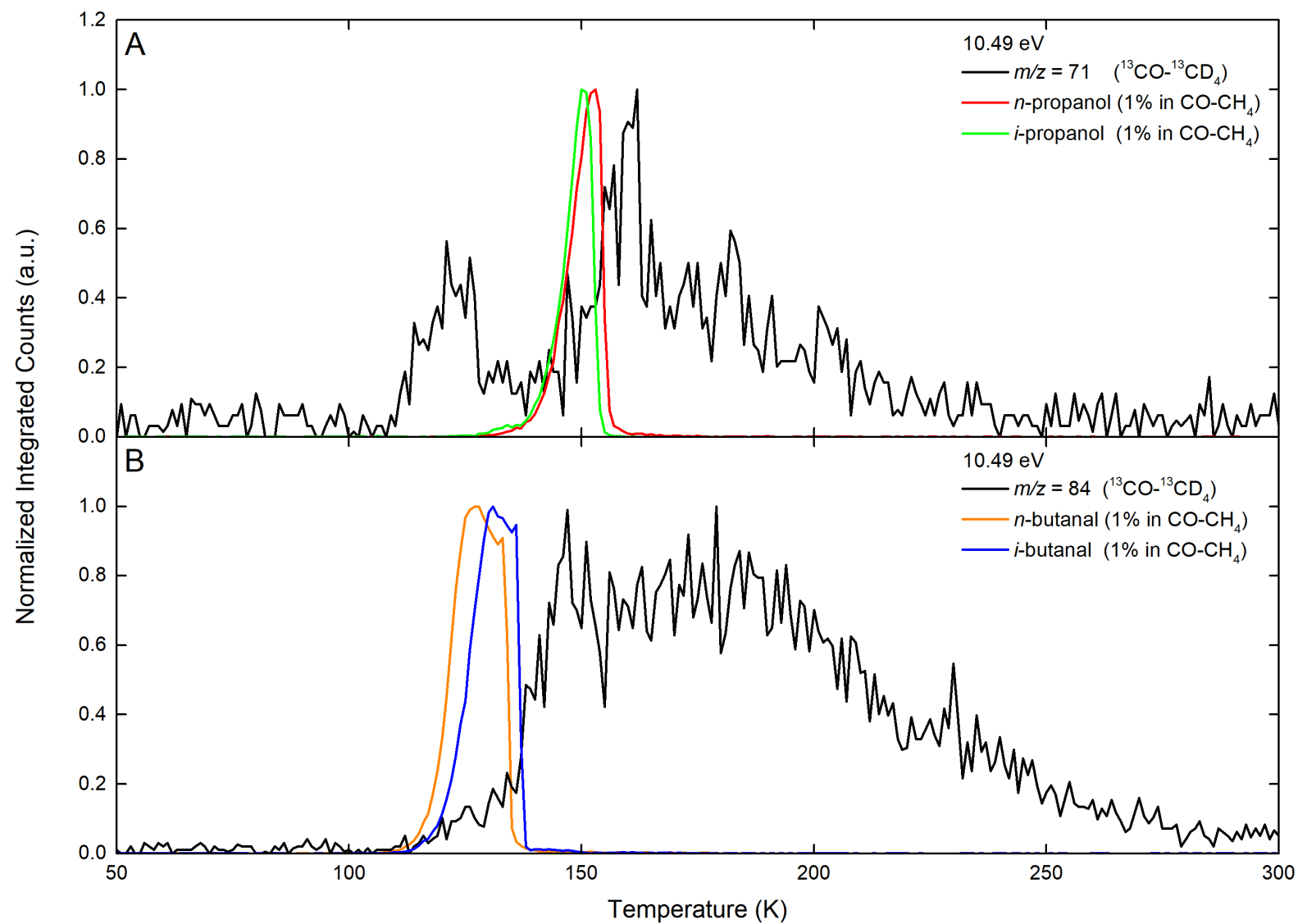


Figure S5. Overlay of PI-ReTOF-MS data (PI = 10.49 eV) recorded for (A) $m/z = 71$ (black) from the irradiated carbon monoxide–methane ice with two possible isomers, n -propanol (red) and i -propanol (green), in 1% calibration experiments and (B) $m/z = 84$ (black) from the irradiated carbon monoxide–methane ice with two possible isomers, n -butanol (orange) and i -butanol (blue), in 1% calibration experiments responsible for the signal.

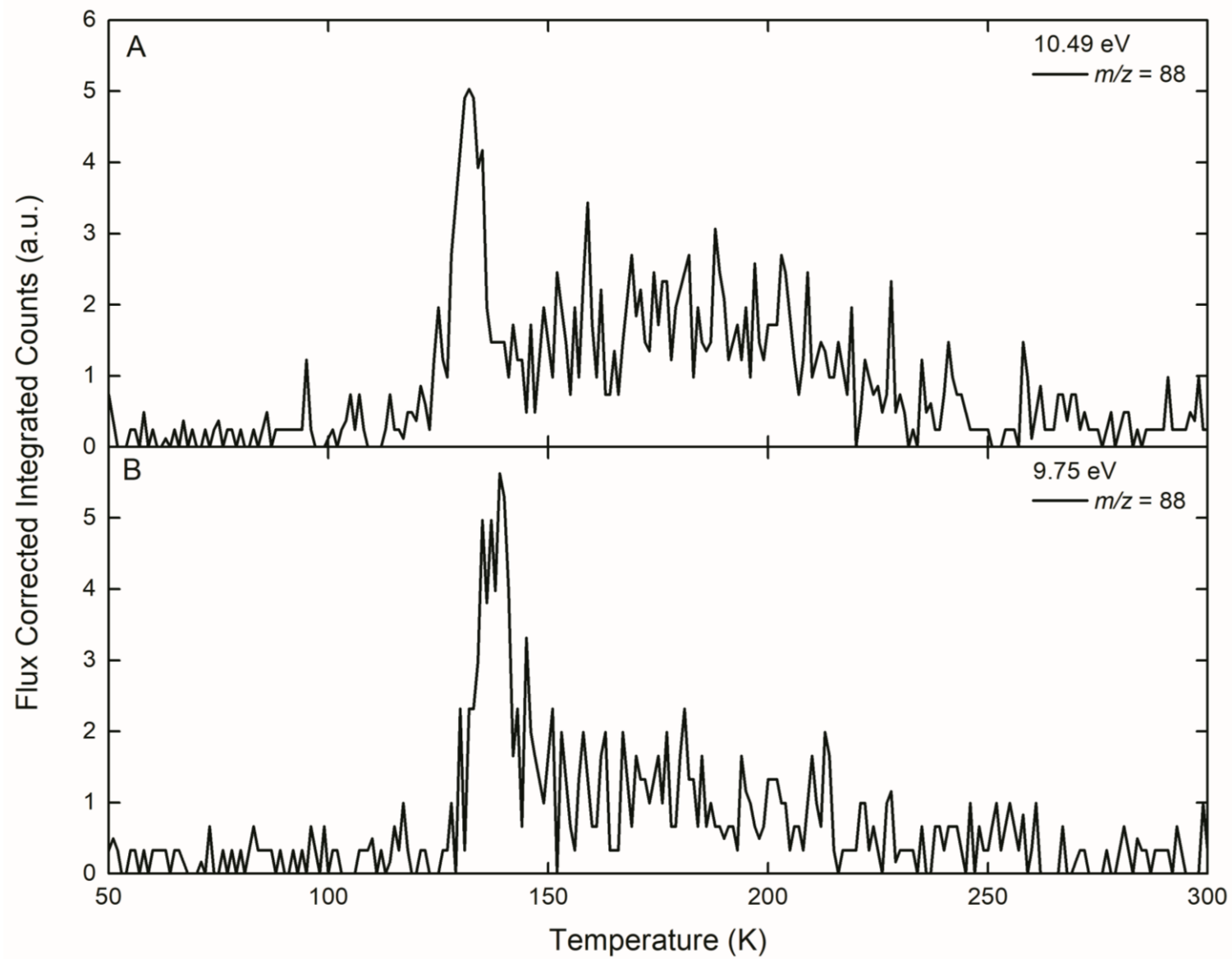


Figure S6. PI-ReTOF-MS data recorded for the ion signal $m/z = 88$ ($^{13}\text{C}_4\text{D}_{10}\text{O}^+$) with PI energies of (A) 10.49 eV and (B) 9.75 eV.

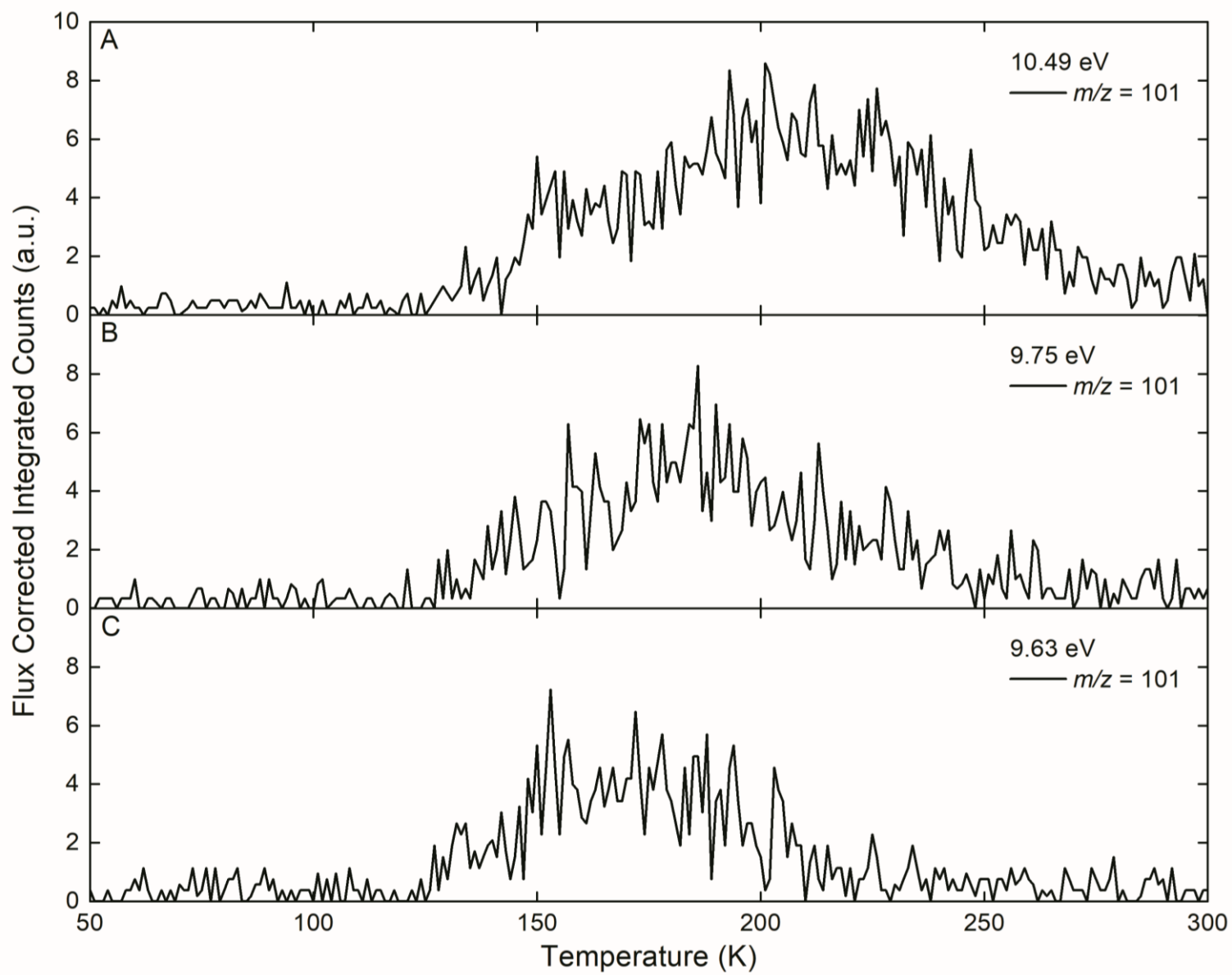


Figure S7. PI-ReTOF-MS data recorded for the ion signal $m/z = 101$ ($^{13}\text{C}_5\text{D}_{10}\text{O}^+$) with PI energies of (A) 10.49 eV, (B) 9.75 eV, and (C) 9.63 eV.

Table S1. List of Experiments

Experiment #	Starting Chemicals	Processing	Photoionization Energy (eV)	Experiment Type	Purpose
1	CO-CH ₄	None used	10.49	PI-ReTOF-MS blank	Control experiment
2	CO-CH ₄	30 nA of 5 keV electrons for 1 hour	-	FTIR analysis during irradiation and TPD	To check for FTIR peaks of interest for C ₃ H ₈ O/C ₄ H ₈ O
3	CO-CH ₄	30 nA of 5 keV electrons for 1 hour	10.49	FTIR analysis during irradiation and PI-ReTOF-MS during TPD	To check for ion signals of interest for C ₃ H ₈ O/C ₄ H ₈ O
4	¹³ CO- ¹³ CD ₄	None used	10.49	PI-ReTOF-MS blank	Control experiment
5	¹³ CO- ¹³ CD ₄	30 nA of 5 keV electrons for 1 hour	10.49	FTIR analysis during irradiation and PI-ReTOF-MS during TPD	To confirm the signals of C ₃ H ₈ O and C ₄ H ₈ O by shifting their signals to the unique <i>m/z</i> 71 (¹³ C ₃ D ₈ O) and <i>m/z</i> 84 (¹³ C ₄ D ₈ O)
6	¹³ CO- ¹³ CD ₄	30 nA of 5 keV electrons for 1 hour	9.92	FTIR analysis during irradiation and PI-ReTOF-MS during TPD	To confirm methy ethyl ether (¹³ C ₃ D ₈ O) and discriminate between ¹³ C ₄ D ₈ O isomers
7	¹³ CO- ¹³ CD ₄	30 nA of 5 keV electrons for 1 hour	9.75	FTIR analysis during irradiation and PI-ReTOF-MS during TPD	To discriminate between ¹³ C ₄ D ₈ O isomers; used to confirm <i>n</i> -butanal
8	¹³ CO- ¹³ CD ₄	30 nA of 5 keV electrons for 1 hour	9.63	FTIR analysis during irradiation and PI-ReTOF-MS during TPD	To discriminate between ¹³ C ₄ D ₈ O isomers; used to confirm <i>i</i> -butanal
9	1% <i>n</i> -propanol (C ₃ H ₈ O) and 1% <i>n</i> -butanal (C ₄ H ₈ O) in CO-CH ₄	None used	10.49; 9.75	FTIR and PI-ReTOF-MS calibration	To calibrate the system so that assignments could be confirmed and yields calculated
10	1% <i>i</i> -propanol (C ₃ H ₈ O) and 1% <i>n</i> -butanal (C ₄ H ₈ O) in CO-CH ₄	None used	10.49	FTIR and PI-ReTOF-MS calibration	To calibrate the system so that assignments could be confirmed and yields calculated
11	1% <i>i</i> -propanol (C ₃ H ₈ O) and 1% <i>i</i> -butanal (C ₄ H ₈ O) in CO-CH ₄	None used	9.75	FTIR and PI-ReTOF-MS calibration	To calibrate the system so that assignments could be confirmed and yields calculated
12	1% <i>i</i> -butanal (C ₄ H ₈ O) in CO-CH ₄	None used	9.63	FTIR and PI-ReTOF-MS calibration	To calibrate the system so that assignments could be confirmed and yields calculated

Table S2. Data applied to calculate the average dose per molecule in the isotopically labeled carbon monoxide (¹³CO) and methane (¹³CD₄) ice.

Initial kinetic energy of the electrons	5 keV	
Irradiation current	30 ± 2 nA	
Total number of electrons	(6.7 ± 0.5) × 10 ¹⁴	
Average kinetic energy of backscattered electrons ^[a]	3.3 ± 0.3 keV	
Fraction of backscattered electrons ^[a]	0.33 ± 0.03	
Average kinetic energy of transmitted electrons ^[a]	1.4 ± 0.3 keV	
Fraction of transmitted electrons ^[a]	0.04 ± 0.02	
Average penetration depth ^[a]	290 ± 20 nm	
Density of the mixed ice	0.94 ± 0.09 g cm ⁻³	
Irradiated area	1.0 ± 0.1 cm ²	
Ice constituent	¹³ CO	¹³ CD ₄
Total molecules processed	(5.7 ± 0.9) × 10 ¹⁷	(7.9 ± 1.2) × 10 ¹⁷
Dose per molecule	4.5 ± 0.9 eV	3.3 ± 0.7 eV

[a] CASINO software calculated values.

Table S3. Infrared absorption features recorded before and after the irradiation of methane-carbon monoxide ices at 5 K.

CH ₄ -CO		Assignment	Carrier	References
Before Irradiation (cm ⁻¹)	After Irradiation (cm ⁻¹)			
4534, 4302, 4204		$\nu_2 + \nu_3, \nu_3 + \nu_4, \nu_1 + \nu_4$ (CH ₄)	combinations	[16]
4248		$2\nu_1$ (CO)	overtone	[17]
	3253	ν_3 (C ₂ H ₂)	CH stretch	[16, 18]
	3151	ν_3 (CH ₃)	CH stretch	[9b, 19]
	3093	ν_9 (C ₂ H ₄)	CH ₂ asymmetric stretch	[16]
3011		ν_3 (CH ₄)	degenerate stretch	[16, 18]
	2978	ν_{10} (C ₂ H ₆)	degenerate stretch	[16, 18]
	2962	ν_1 (C ₂ H ₆)	CH ₃ symmetric stretch	[16, 18]
	2943	$\nu_8 + \nu_{11}$ (C ₂ H ₆)	combination	[16, 18]
	2920	$\nu_8 + \nu_{11}$ (C ₂ H ₆)	combination	[16, 18]
2905		ν_1 (CH ₄)	asymmetric stretch	[16, 18]
	2885	ν_5 (C ₂ H ₆)	CH ₃ symmetric stretch	[16, 18]
2818		$\nu_2 + \nu_4$ (CH ₄)	combination	[16, 18]
	2748	$\nu_2 + \nu_6$ (C ₂ H ₆)	combination	[16, 18]
2595		$2\nu_4$ (CH ₄)	overtone	[16, 18]
	2341	ν_3 (CO ₂)	CO asymmetric stretch	[19]
	2276	ν_3 (¹³ CO ₂)	CO asymmetric stretch	[19]
2137		ν_1 (CO)	CO stretch	[17, 19]
2090		ν_1 (¹³ CO)	CO stretch	[17]
	1853	ν_2 (HCO)	CO stretch	[15a]
	1746-1660	[a]	CO stretch	[15a, 20]
	1466	ν_{11} (C ₂ H ₆)	CH ₃ deformation	[16, 18]
	1427	ν_{12} (CH ₃ CHO)	CH ₃ deformation	[15a]
	1373	ν_6 (C ₂ H ₆)	CH ₃ symmetric deformation	[16, 18]
	1350	ν_7 (CH ₃ CHO)	CH ₃ deformation	[15a]
1302		ν_4 (CH ₄)	degenerate stretch	[16, 18]
	1120	ν_8 (CH ₃ CHO)	CH ₃ deformation	[15a]
	1091	ν_2 (HCO)	bending	[15a]
	613	ν_2 (CH ₃)	out of plane	[16, 18]
¹³ CD ₄ - ¹³ CO		Assignment	Carrier	References
Before Irradiation (cm ⁻¹)	After Irradiation (cm ⁻¹)			
4154		$2\nu_1$ (¹³ CO)	overtone	[21]
3216, 3078		$\nu_3 + \nu_4, \nu_1 + \nu_4$ (¹³ CD ₄)	combinations	[16, 22]
	2276	ν_3 (¹³ CO ₂)	CO asymmetric stretch	[21, 23]
2259		ν_3 (CD ₄)	degenerate stretch	[16, 18, 22]
2237		ν_3 (¹³ CD ₄)	degenerate stretch	[16, 18, 22]
	2214	ν_{10} (¹³ C ₂ D ₆)	degenerate stretch	[24]
	2203	$\nu_2 + \nu_8$ (¹³ C ₂ D ₆)	combination	[25]
	2185	ν_1 (¹³ C ₂ D ₆)	CD ₃ symmetric stretch	[26]
	2177	ν_{11} (¹³ C ₂ D ₄)	CD ₂ symmetric stretch	[27]
2137		ν_1 (CO)	CO stretch	[19, 21]
2090		ν_1 (¹³ CO)	CO stretch	[21]
	2073	ν_5 (C ₂ D ₆)	CD ₃ symmetric stretch	[24b]
2063		$\nu_2 + \nu_4$ (CD ₄)	combination	[22b]
	2055	ν_5 (¹³ C ₂ D ₆)	CD ₃ symmetric stretch	[24b]
	2051	ν_2 (¹³ CD ₂ ¹³ CO)	CO stretch	[15e, 28]
2038		$\nu_2 + \nu_4$ (¹³ CD ₄)	combination	[22b]
	2026	$\nu_6 + \nu_9$ (¹³ C ₂ D ₆)	combination	[24a, 26, 29]
1962		$2\nu_4$ (¹³ CD ₄)	overtone	[22b]
	1774	ν_3 (D ¹³ CO)	CO stretch	[30]
	1682-1663	[a]	CO stretch	[30]
	1067	ν_{12} (¹³ C ₂ D ₄)	CD ₂ symmetric stretch	[27]
985		ν_4 (¹³ CD ₄)	degenerate stretch	[16, 18, 22]

[a] Carbonyl stretching region (saturated/unsaturated aldehydes/ketones with mono-/di-/tri-/tetra- substituted side chains).

Table S4. Yield of Selected COMs.

<i>m/z</i>	Name	Formula	IE (eV)	Photoionization Cross Section (Mb)	Yield (Molecules eV ⁻¹)	References
71	<i>n</i> -propanol	¹³ C ₃ D ₈ O	10.22 ± 0.06	3.385 (10.49 eV)	^a 2.2 ± 0.9 × 10 ⁻⁴	[14]
71	<i>i</i> -propanol	¹³ C ₃ D ₈ O	10.10 ± 0.02	0.61 (10.49 eV)	^a 1.2 ± 0.5 × 10 ⁻³	[14]
71	methyl ethyl ether	¹³ C ₃ D ₈ O	9.72 ± 0.07	10.7 (10.49 eV) 4.291 (9.93 eV) 1.255 (9.75 eV)	2.1 ± 0.9 × 10 ⁻⁵	[31]
84	<i>n</i> -butanal	¹³ C ₄ D ₈ O	9.82 ± 0.04	9.018 (10.49 eV) 3.7175 (9.93 eV) 0.027 (9.75 eV)	2.0 ± 0.8 × 10 ⁻⁴	[32]
84	<i>i</i> -butanal	¹³ C ₄ D ₈ O	9.71 ± 0.02	12.033 (10.49 eV) 6.7145 (9.93 eV) 1.68 (9.75 eV)	1.3 ± 0.5 × 10 ⁻⁴	[32]

[a] Upper limit due to the overlap of ionization energies and sublimation temperatures of *n*- and *i*-propanol.

Table S5. Reaction Energies.

Reaction	Reaction	$\Delta_R G^{[a]}$	
		kJ mol^{-1}	eV
S1	$\text{CO} (X^1\Sigma^+) + \text{CH}_4 (X^1A_1) \rightarrow \text{CH}_3\text{CHO} (X^1A')$	20	0.21
S2	$\text{CO} (X^1\Sigma^+) + \text{C}_2\text{H}_6 (X^1A_1) \rightarrow \text{CH}_3\text{CH}_2\text{CHO} (X^1A')$	12	0.12
S3	$\text{CH}_4 (X^1A_1) \rightarrow \text{CH}_3 (X^2A_2'') + \text{H} (^2S_{1/2})$	429	4.44
S4	$\text{H} (^2S_{1/2}) + \text{CO} (X^1\Sigma^+) \rightarrow \text{HCO} (X^2A')$	-57	-0.59
S5	$\text{C}_2\text{H}_6 (X^1A_{1g}) \rightarrow \text{C}_2\text{H}_5 (X^2A') + \text{H} (^2S_{1/2})$	412	4.27
S6	$\text{C}_3\text{H}_8 (X^1A_1) \rightarrow n\text{-C}_3\text{H}_7 (X^2A'') + \text{H} (^2S_{1/2})$	395	4.10
S7	$\text{C}_3\text{H}_8 (X^1A_1) \rightarrow i\text{-C}_3\text{H}_7 (X^2A') + \text{H} (^2S_{1/2})$	381	3.95
S8	$\text{HCO} (X^2A') + \text{CH}_3 (X^2A_2'') \rightarrow \text{CH}_3\text{CHO} (X^1A')$	-352	-3.65
S9	$\text{HCO} (X^2A') + \text{C}_2\text{H}_5 (X^2A') \rightarrow \text{CH}_3\text{CH}_2\text{CHO} (X^1A')$	-344	-3.57
S10	$\text{HCO} (X^2A') + n\text{-C}_3\text{H}_7 (X^2A'') \rightarrow \text{CH}_3\text{CH}_2\text{CH}_2\text{CHO} (X^1A')$	-328	-3.40
S11	$\text{HCO} (X^2A') + i\text{-C}_3\text{H}_7 (X^2A') \rightarrow (\text{CH}_3)_2\text{CHCHO} (X^1A')$	-344	-3.56
S12	$\text{CH}_3\text{CHO} (X^1A') + 2\text{H} (^2S_{1/2}) \rightarrow \text{CH}_3\text{CH}_2\text{OH} (X^2A')$	-481	-4.98
S13	$\text{CH}_3\text{CH}_2\text{CHO} (X^1A') + 2\text{H} (^2S_{1/2}) \rightarrow \text{CH}_3\text{CH}_2\text{CH}_2\text{OH} (X^1A')$	-485	-5.02
S14	$\text{CH}_3\text{CHO} (X^1A') \rightarrow \text{CH}_3\text{CO} (X^2A') + \text{H} (^2S_{1/2})$	369	3.82
S15	$\text{CH}_3\text{CO} (X^2A') + \text{CH}_3 (X^2A_2'') \rightarrow (\text{CH}_3)_2\text{CO} (X^1A_1)$	-347	-3.59
S16	$(\text{CH}_3)_2\text{CO} (X^1A_1) + 2\text{H} (^2S_{1/2}) \rightarrow (\text{CH}_3)_2\text{CHOH} (X^1A)$	-472	-4.89
S17	$\text{HCO} (X^2A') + 2\text{H} (^2S_{1/2}) \rightarrow \text{CH}_3\text{O} (X^2A')$	-437	-4.53
S18	$\text{CH}_3\text{O} (X^2A') + \text{C}_2\text{H}_5 (X^2A') \rightarrow \text{CH}_3\text{OCH}_2\text{CH}_3 (X^1A')$	-354	-3.67
S19	$\text{CH}_3\text{CH}_2\text{OH} (X^2A') \rightarrow \text{CH}_3\text{CH}_2\text{O} (X^2A') + \text{H} (^2S_{1/2})$	429	4.45
S20	$\text{CH}_3\text{CH}_2\text{O} (X^2A') + \text{CH}_3 (X^2A_2'') \rightarrow \text{CH}_3\text{OCH}_2\text{CH}_3 (X^1A')$	-343	-3.56
S21	$\text{CO} (X^1\Sigma^+) \rightarrow \text{C} (^3P) + \text{O} (^1D)$	1260	13.07
S22	$\text{C}_3\text{H}_8 (X^1A_1) + \text{O} (^1D) \rightarrow \text{CH}_3\text{CH}_2\text{CH}_2\text{OH} (X^1A')$	-586	-6.07
S23	$\text{C}_3\text{H}_8 (X^1A_1) + \text{O} (^1D) \rightarrow (\text{CH}_3)_2\text{CHOH} (X^1A)$	-603	-6.25
S24	$\text{C}_3\text{H}_8 (X^1A_1) + \text{O} (^1D) \rightarrow \text{CH}_3\text{CH}_2\text{OCH}_3 (X^1A')$	-548	-5.68

[a] see <http://webbook.nist.gov/chemistry>.

Table S6. Theoretical and Experimental Branching Ratios for $\text{C}_3\text{H}_8\text{O}$ and $\text{C}_4\text{H}_8\text{O}$ Isomers.

Isomers	ΔG (kJ mol^{-1})	Theoretical Thermal Equilibrium Ratio		Experimental Ratio
		K (at 10 K)	K (at 200 K)	
<i>i</i> -propanol : <i>n</i> -propanol	-17 ± 3	$2.3 \pm 0.4 \times 10^{30}$	$3.3 \pm 0.6 \times 10^4$	6 ± 3
<i>n</i> -propanol : methyl ethyl ether	-38 ± 3	$8.5 \pm 0.7 \times 10^{196}$	$7.0 \pm 0.6 \times 10^9$	11 ± 6
<i>i</i> -propanol : methyl ethyl ether	-55 ± 1	$2.0 \pm 0.1 \times 10^{287}$	$2.3 \pm 0.1 \times 10^{14}$	57 ± 32
<i>i</i> -butanal : <i>n</i> -butanal	-30 ± 1	$1.9 \pm 0.1 \times 10^{157}$	$7.3 \pm 0.3 \times 10^7$	0.7 ± 0.3

References

- [1] M. J. Abplanalp, A. Borsuk, B. M. Jones, R. I. Kaiser, *Astrophys. J.* **2015**, *814*, 45-61.
- [2] A. M. Goodman, *Appl. Opt.* **1978**, *17*, 2779-2787.
- [3] A. C. A. Boogert, P. A. Gerakines, D. C. B. Whittet, *Annu. Rev. Astron. Astrophys.* **2015**, *53*, 541-581.
- [4] D. Drouin, A. R. Couture, D. Joly, X. Tastet, V. Aimez, R. Gauvin, *Scanning* **2007**, *29*, 92-101.
- [5] G. J. Jiang, W. B. Person, K. G. Brown, *J. Chem. Phys.* **1975**, *62*, 1201-1211.
- [6] M. Á. Satorre, M. Domingo, C. Millán, R. Luna, R. Vilaplana, C. Santonja, *Planet. Space Sci.* **2008**, *56*, 1748-1752.
- [7] A. I. Prokhvatilov, A. P. Isakina, *Phys. Status Solidi A* **1983**, *78*, 147-155.
- [8] E. Herbst, *Int. Rev. Phys. Chem.* **2017**, *36*, 287-331.
- [9] a) M. J. Abplanalp, S. Gozem, A. I. Krylov, C. N. Shingledecker, E. Herbst, R. I. Kaiser, *Proc. Natl. Acad. Sci. U. S. A.* **2016**, *113*, 7727-7732; b) M. J. Abplanalp, M. Förstel, R. I. Kaiser, *Chem. Phys. Lett.* **2016**, *644*, 79-98.
- [10] R. Hilbig, R. Wallenstein, *IEEE J. Quantum Electron.* **1981**, *17*, 1566-1573.
- [11] R. Hilbig, G. Hilber, A. Lago, B. Wolff, R. Wallenstein, in *Nonlinear Optics and Applications, Vol. 613* (Ed.: P. Yeh), SPIE-The International Society for Optical Engineering, **1986**, pp. 48-55.
- [12] A. Bergantini, P. Maksyutenko, R. I. Kaiser, *Astrophys. J.* **2017**, *841*, 96.
- [13] A. M. Turner, M. J. Abplanalp, S. Y. Chen, Y. T. Chen, A. H. H. Chang, R. I. Kaiser, *Phys. Chem. Chem. Phys.* **2015**, *17*, 27281-27291.
- [14] T. A. Cool, J. Wang, K. Nakajima, C. A. Taatjes, A. McIlroy, *International Journal of Mass Spectrometry* **2005**, *247*, 18-27.
- [15] a) C. J. Bennett, C. S. Jamieson, Y. Osamura, R. I. Kaiser, *Astrophys. J.* **2005**, *624*, 1097-1115; b) C. J. Bennett, Y. Osamura, M. D. Lebar, R. I. Kaiser, *Astrophys. J.* **2005**, *634*, 698-711; c) C. J. Bennett, R. I. Kaiser, *Astrophys. J.* **2007**, *661*, 899-909; d) L. Zhou, R. I. Kaiser, L. G. Gao, A. H. H. Chang, M. C. Liang, Y. L. Yung, *Astrophys. J.* **2008**, *686*, 1493-1502; e) S. Maity, R. I. Kaiser, B. M. Jones, *Astrophys. J.* **2014**, *789*, 36; f) S. Maity, R. I. Kaiser, B. M. Jones, *Faraday Discuss.* **2014**, *168*, 485; g) M. Förstel, P. Maksyutenko, B. M. Jones, B. J. Sun, H. C. Lee, A. H. H. Chang, R. I. Kaiser, *Astrophys. J.* **2016**, *820*, 117.
- [16] C. J. Bennett, C. S. Jamieson, Y. Osamura, R. I. Kaiser, *Astrophys. J.* **2006**, *653*, 792-811.
- [17] C. S. Jamieson, A. M. Mebel, R. I. Kaiser, *Astrophys. J., Suppl. Ser.* **2006**, *163*, 184-206.
- [18] R. I. Kaiser, K. Roessler, *Astrophys. J.* **1998**, *503*, 959-975.
- [19] C. J. Bennett, C. Jamieson, A. M. Mebel, R. I. Kaiser, *Phys. Chem. Chem. Phys.* **2004**, *6*, 735-746.
- [20] a) G. A. Guirgis, B. R. Drew, T. K. Gounev, J. R. Durig, *Spectrochim. Acta, Part A* **1998**, *54*, 123-143; b) W. Coleman, B. M. Gordon, *Appl. Spectrosc.* **1987**, *41*, 1169-1172; c) G. Socrates, *Infrared and Raman characteristic group frequencies: tables and charts*, John Wiley & Sons, **2004**; d) W. Coleman, B. M. Gordon, *Appl. Spectrosc.* **1987**, *41*, 1159-1162; e) X. K. Zhang, E. G. Lewars, R. E. March, J. M. Parnis, *JPC* **1993**, *97*, 4320-4325.
- [21] C. J. Bennett, C. S. Jamieson, R. I. Kaiser, *Phys. Chem. Chem. Phys.* **2009**, *11*, 4210-4218.
- [22] a) J. He, K. Gao, G. Vidali, C. J. Bennett, R. I. Kaiser, *Astrophys. J.* **2010**, *721*, 1656; b) P. Calvani, S. Lupi, P. Maselli, *J. Chem. Phys.* **1989**, *91*, 6737-6742.
- [23] C. J. Bennett, C. Jamieson, S., R. Kaiser, I., *Astrophys. J., Suppl. Ser.* **2009**, *182*, 1-11.
- [24] a) I. M. Nyquist, I. M. Mills, W. B. Person, B. Crawford, *J. Chem. Phys.* **1957**, *26*, 552-558; b) M. G. Wisnosky, D. F. Eggers, L. R. Fredrickson, J. C. Decius, *J. Chem. Phys.* **1983**, *79*, 3513-3516.
- [25] S. B. Tejada, D. F. Eggers, *Spectrochim. Acta, Part A* **1976**, *32*, 1557-1562.
- [26] M. J. Abplanalp, R. I. Kaiser, *Astrophys. J.* **2016**, *827*, 132.
- [27] M. E. Jacox, *J. Chem. Phys.* **1962**, *36*, 140-143.
- [28] R. L. Hudson, M. J. Loeffler, *Astrophys. J.* **2013**, *773*, 109.
- [29] S. Kondo, S. Saëki, *Spectrochim. Acta, Part A* **1973**, *29*, 735-751.
- [30] R. I. Kaiser, S. Maity, B. M. Jones, *Phys. Chem. Chem. Phys.* **2014**, *16*, 3399-3424.
- [31] H. Koizumi, *J. Chem. Phys.* **1991**, *95*, 5846-5852.
- [32] B. Yang, J. Wang, T. A. Cool, N. Hansen, S. Skeen, D. L. Osborn, *Int. J. Mass Spectrom.* **2012**, *309*, 118-128.